Molecular imaging applications of antibody-based immunotherapeutics to understand cancer drug distribution

Waaijer, Stijn

DOI:
10.33612/diss.144614649

3

Biodistribution and PET Imaging of Labeled Bispecific T Cell Engaging Antibody Targeting EpCAM

Frank J. Warnders[1], Stijn J.H. Waaijer[2*], Martin Pool[2*], Marjolijn N. Lub-de Hooge[1,3], Matthias Friedrich[4], Anton G.T. Terwisscha van Scheltinga[1], Petra Deegen[4], Sabine K. Stienen[4], Pete C. Pieslor[5], Hung K. Cheung[5], Jos G.W. Kosterink[1,6], Elisabeth G.E. de Vries[2]

[1]Department of Clinical Pharmacy and Pharmacology, University Medical Center Groningen, University of Groningen, Groningen, The Netherlands, [2]Department of Medical Oncology, University Medical Center Groningen, University of Groningen, Groningen, The Netherlands, [3]Department of Nuclear Medicine and Molecular Imaging, University Medical Center Groningen, University of Groningen, Groningen, The Netherlands, [4] Amgen Research (Munich) GmbH, Germany, [5] Amgen, Thousand Oaks, CA; USA, [6] Department of Pharmacy, Section of Pharmacotherapy and Pharmaceutical Care, University of Groningen, Groningen, The Netherlands

[*] both authors contributed equally to this work.

J Nucl Med 2016;57(5):812-857

ABSTRACT

AMG 110, a bispecific T cell engager (BiTE) antibody construct, induces T cell mediated cancer cell death by cross-linking epithelial cell adhesion molecule (EpCAM) on tumor cells with cluster of differentiation 3 epsilon (CD3ε) on T cells. We labeled AMG 110 with zirconium-89 (^{89}Zr) or near infrared fluorescent dye (IRDye) 800CW to study its tumor targeting and tissue distribution.

Biodistribution and tumor uptake of ^{89}Zr-AMG 110 was studied up to 6 days after intravenous injection in nude BALB/c mice bearing high EpCAM expressing HT-29 colorectal cancer xenografts. Tumor uptake of ^{89}Zr-AMG 110 was compared with uptake in head and neck squamous cell cancer FaDu (intermediate EpCAM) and promyelocytic leukemia HL60 (EpCAM negative) xenografts. Intratumoral distribution in HT-29 tumors was studied using 800CW-AMG 110.

Tumor uptake of ^{89}Zr-AMG 110 can be clearly visualized using small-animal PET imaging up to 72 h after injection. Highest tumor uptake of ^{89}Zr-AMG 110 at a 40 μg dose level of was observed at 6 h and 24 h (respectively 5.35 ± 0.22 %ID/g and 5.30 ± 0.20 %ID/g; n = 3 and n = 4). Tumor uptake of ^{89}Zr-AMG 110 was EpCAM specific and correlated with EpCAM expression. 800CW-AMG 110 accumulated at the tumor cell surface in viable EpCAM expressing tumor tissue.

PET and fluorescent imaging provided real-time information about AMG 110 distribution and tumor uptake *in vivo*. Our data support using ^{89}Zr and IRDye 800CW to evaluate tumor and tissue uptake kinetics of BITE antibody constructs in preclinical and clinical settings.

INTRODUCTION

Cancer remains a major cause of death worldwide and one of the key disease areas with the greatest unmet medical needs. Therefore, new treatment strategies are eagerly awaited. The use of T cells, especially cytotoxic T cells, in the battle against cancer has shown promising results using several approaches.[1] However, most of these strategies are sensitive to inhibitory or escape mechanisms, such as major histocompatibility complex class I downregulation or induction of T cell tolerance, which can limit antitumor efficacy.[2,3]

Bispecific T cell engager (BiTE) antibody constructs are created to circumvent such inhibitory or escape mechanisms. They are comprised of 2 single-chain variable antibody fragments (scFv) that are covalently linked by a peptide linker and bind cluster of differentiation 3 ε (CD3ε) as well as a surface target antigen on cancer cells.[4] The activation of T cells by BiTE antibody constructs is independent of matching major histocompatibility complex class I or costimulatory molecules.[5,6] Furthermore, BiTE antibody constructs engage a polyclonal population of T cells, including $CD4^+$ and mainly $CD8^+$ T cells.[7]Binding of tumor cells and T cells by BiTE antibody constructs results in the formation of a cytolytic synapse between tumor and T cells, which is followed by a release of pore-forming and pro-apoptotic components of cytotoxic T cell granules, mediating cancer cell death.[5,7] The activation of T cells occurs only in the presence of a target cell.[8] To date, four BiTE antibody constructs, blinatumomab, BAY2010112/AMG 212, MT111/AMG 211 and MT110/AMG 110 are or have been tested in clinical trials. Blinatumomab has been approved by the U.S. Food and Drug Administration to treat patients with Philadelphia chromosome-negative precursor B-cell acute lymphoblastic leukemia.

Epithelial cell adhesion molecule (EpCAM) is expressed on many epithelial tumors and cancer stem cells[9] and is therefore an attractive target for BiTE antibody constructs. An EpCAM targeting BiTE called solitomab (AMG 110, formerly known as MT110) has been developed.[10]AMG 110 mediates lysis of cancer cells by the activation of T cells *in vitro* and showed pharmacological activity at doses administered of at least 24 μg/day in the clinic.[11]

To support clinical development of AMG 110 and other BiTE antibody constructs, molecular imaging can be used as a powerful noninvasive tool to obtain valuable information on tumor uptake, biodistribution, and pharmacokinetics. In a clinical setting, this information can potentially be used to support patient-tailored drug dosing. Because of its long radioactivity decay half-life of 3.27 d, zirconium-89 (^{89}Zr) is well suited for capturing the *in vivo* pharmacokinetics of large molecules, such as antibodies.[12] In addition, labeling antibodies with the near infrared (NIR) fluorescent dye 800CW can be used to study their intratumoral tumor distribution with near infrared fluorescence imaging and to enable molecular characterization of tumor and tissue sections *ex vivo*.[13] We therefore labeled AMG 110 with ^{89}Zr or IRDye 800CW to study its tumor targeting and tissue distribution via noninvasive small-animal positron emission tomography (PET) and fluorescence imaging.

MATERIALS AND METHODS

BiTE antibody constructs and cell lines

AMG 110 is a BiTE antibody construct targeting human EpCAM and human CD3ε. The nonspecific control BiTE Mec14 shares the same anti-CD3ε single-chain antibody arm but targets a haptene (mecoprop) with the second arm. Both BiTE antibody constructs, ± 55 kDa in size, were provided by Amgen. Two human EpCAM-positive tumor cell lines, the colorectal adenocarcinoma HT-29 cell line and the head and neck squamous cell cancer FaDu cell line, and a human EpCAM-negative promyelocytic leukemia HL-60 cell line were used. We used HT-29 xenografts to study dose- and time-dependent tumor uptake of ^{89}Zr-AMG110 as this cell line highly expresses EpCAM.[14] We additionally used this cell line to compare EpCAM-dependent tumor uptake of ^{89}Zr-AMG110 with ^{89}Zr-Mec14. All cell lines were obtained from American Type Culture Collection and screened for microbial contamination and tested negative. Cell lines were authenticated by Baseclear using short tandem repeat profiling. This was repeated once a cell line has been passaged for more than 6 months after previous short tandem repeat profiling. HT-29 and HL-60 were routinely cultured in RPMI-1640 medium (Invitrogen) containing 10% fetal calf serum (Bodinco BV). FaDu cells were cultured in DMEM (Invitrogen) supplemented with 10% fetal calf serum and 2 mM L-glutamine (Invitrogen). All cells were cultured under humidified conditions (37°C, 5% CO2).

Animal experiments

All animal experiments were approved by the Institutional Animal Care and Use Committee of the University of Groningen and conducted in male nude BALB/c mice (BALB/cOlaHsd-Foxn1^{nu}, Harlan). After 1 week of acclimatization, 6- to 8-wk-old mice were subcutaneously injected with 10 x 10^6 HT-29 cells in 0.1 mL phosphate-buffered saline, 5 x 10^6 FaDu cells in 0.1 mL phosphate-buffered saline or 2 x 10^6 HL-60 cells in 0.1 mL phosphate-buffered saline. Tumor growth was monitored by caliper measurements. Penile vein tracer injection was performed 3 wk after inoculation of HT-29 cells, 4 wk after inoculation of FaDu cells and 5 wk after inoculation for HL-60 cells. All scans and invasive proceedings were performed with isoflurane/medical air inhalation anesthesia (5% induction, 2.5% maintenance) for a maximum of 90 min.

PET acquisition

Two mice were placed above each other in a Focus 220 rodent scanner (CTI Siemens), with the tumor in field of view. Mice were kept warm on heating mats. Acquisition times differed between 10 min (0.5-h time point) and 75 minutes (144-h time point). A transmission scan of 515 seconds was performed using a ^{57}Co point source to correct for tissue attenuation.

In vivo PET imaging and *ex vivo* biodistribution

For determining the time point for optimal tumor visualization, small-animal PET images were obtained 0.5, 3, 6, 24, 48 and 72 h after injection of 20 μg ^{89}Zr-AMG 110 (5 MBq). Data up to 24 h was obtained from 6 mice and data at 48 h and 72 h were obtained from 2 mice. For *ex vivo* biodistribution, animals were sacrificed at designated time points. Subsequently, organs and tissues were excised and weighed. Samples and prime standards were counted for radioactivity in a calibrated well-type γ-counter. *Ex vivo* tissue activity was expressed as percentage of the injected dose per gram tissue (%ID/g). A dose escalation biodistribution study was performed with 20 (n = 5), 40 (n = 4) and 500 μg (n = 3) ^{89}Zr-AMG 110 (1 MBq) at 24 h post injection. Tumor weights did not differ significantly between the dose groups (0.23 ± 0.09, 0.33 ± 0.27 and 0.47 ± 0.62 g, respectively; Supplementary Fig. 1A). Doses higher than 20 μg were supplemented with nonradiolabeled AMG 110. For the 40-μg protein dose, ^{89}Zr-AMG 110 (1 MBq) time-dependent tumor uptake was also determined. Biodistribution studies were performed at 6 (n = 3), 24 (n = 4), 72 (n = 4) and 144 (n = 5) h after tracer injection. Tumor weights did not differ significantly between different groups (0.20 ± 0.01 g, 0.33 ± 0.27 g, 0.33 ± 0.10 g and 0.35 ± 0.15 g, respectively; Supplementary Fig. 1B).

To determine nonspecific tumor uptake, 40 μg (1 MBq) of ^{89}Zr-Mec14 (n = 6) or ^{89}Zr-AMG 110 (n = 4) were administered intravenously to mice harboring HT-29 tumors. Tumor weights did not differ significantly between the 2 groups (0.32 ± 0.11 g and 0.33 ± 0.27 g, respectively; Supplementary Fig. 1C). Small-animal PET scans and *ex vivo* biodistribution were performed 24 h after tracer injection; at the time when tumor uptake of ^{89}Zr-AMG 110 would be high and blood levels relatively low. The biologic half-life of ^{89}Zr-AMG 110 in whole blood and tumor was calculated using either %ID per cubic centimeter (%ID/cm^3) (20-μg tracer dose, as used for determining optimal time point) based on small-animal PET scans or %ID/g (40-μg protein dose) by nonlinear regression (1-phase exponential decay) using GraphPad Prism (GraphPad Software).

EpCAM-specific uptake in relation to EpCAM expression was assessed with small-animal PET imaging 24 h after injection of 40 μg of ^{89}Zr-AMG 110 in xenografted mice (n = 4-6 per group) bearing HT-29, FaDu or HL-60 tumors. Thereafter, mice were sacrificed for *ex vivo* biodistribution analysis. Tumor weights did not differ significantly between the tumor models (0.33 ± 0.27 g, 0.20 ± 0.13 g and 0.34 ± 0.10 g, respectively; Supplementary Fig. 1D).

PET reconstruction

PET data were reconstructed by using a 2-dimensional ordered subset expectation maximization reconstruction algorithm with Fourier rebinning, 4 iterations and 16 subsets. After reconstruction, images were quantified using AMIDE Medical Image Data Examiner software (version 1.0.4; Stanford University). Regions of interest were drawn for tumor and blood (heart). The level of ^{89}Zr-AMG 110 or ^{89}Zr-Mec14 was calculated as %ID/cm^3.

Ex vivo fluorescent imaging

For NIR fluorescence imaging, mice bearing HT-29 xenografts ($n = 4$) were coinjected with 40 µg 800CW-AMG 110 and 40 µg 680RD-Mec14. At 24 h after injection mice were sacrificed, tumor tissue was excised, formalin-fixed and paraffin-embedded. Tumor slices were stained immunohistochemically for EpCAM (D9S3P, Cell Signaling) and with hematoxylin and eosin. Overview images of intratumoral 680RD-Mec14 and 800CW-AMG 110 distribution were obtained with the Odyssey infrared imaging system (LI-COR Biosciences). For fluorescence microscopy, an inverted Leica DMI600B fluorescence microscope equipped with a Lumen Dynamics X-Cite 200DC light source was used. Nuclei were stained with 4',6-diamidino-2-phenylindole (DAPI, Sigma-Aldrich).

Statistical analysis

Data are presented as mean ± SD. Statistical analysis between 2 groups was performed using Mann-Whitney *U* test (GraphPad Prism 5). To test whether differences between multiple groups were significant, we used a Kruskal-Wallis test (GraphPad, Prism 5). A Bonferroni-corrected Mann-Whitney *U* test was subsequently used to compare differences between 2 groups. *P* values of 0.05 or less were considered significant.

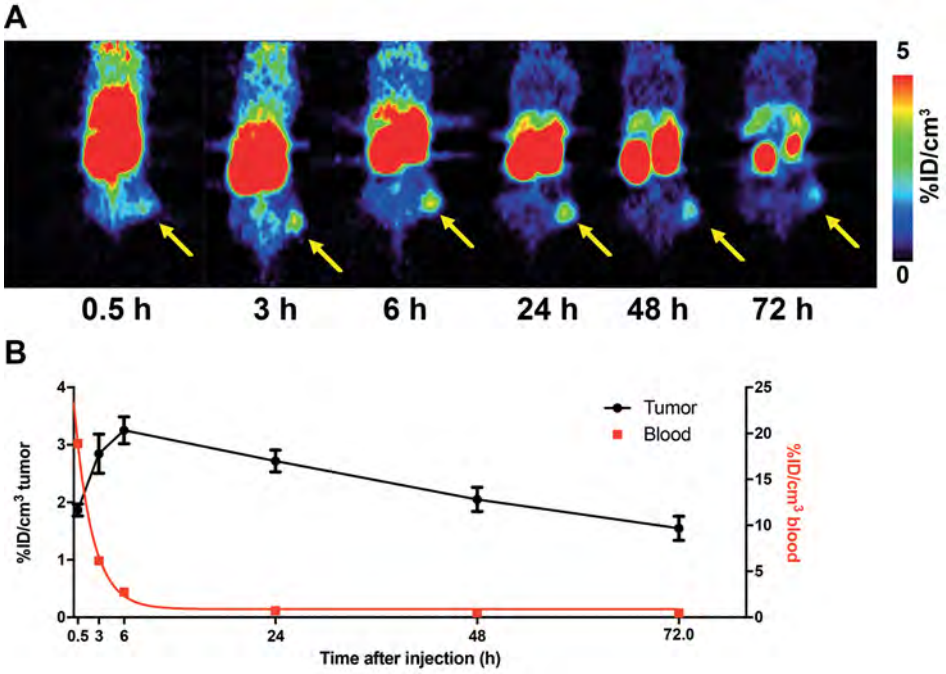

FIGURE 1.

Biodistribution of ^{89}Zr-AMG 110 at a 20 µg dose level. (**A**) Representative serial small-animal PET imaging at 0.5, 3, 6, 24, 48, and 72 h after injection, in one HT-29 bearing mouse. Yellow arrows indicate the tumor. (**B**) *In vivo* quantification of tumor and blood levels of ^{89}Zr-AMG 110 in time as presented in %ID/cm^3. Data up to 24 h was obtained from 6 mice and data at 48 h and 72 h were obtained from 2 mice. Data are presented as mean ± SD.

RESULTS

In vivo evaluation of ^{89}Zr-AMG 110 and 800CW-AMG 110

Small-animal PET images of the 20-µg ^{89}Zr-AMG 110 dose showed time-dependent tumor accumulation with a maximum of 3.25 ± 0.24 %ID/cm^3 at 6 h after injection (Figs. 1A and 1B) and decreasing subsequently. Following the same pattern, kidneys showed the highest tissue uptake across time points, reaching a maximum of 60.26 ± 4.01 %ID/cm^3 at 6 h, indicating renal clearance. Blood levels of ^{89}Zr-AMG 110 dropped rapidly (biological half-life, 1.51 h: Supplementary Fig. 4A). The washout of the tumor was relatively slow (biological half-life, 99.9 h: Supplementary Fig. 4B), starting at 6 h after injection. This resulted in increasing tumor-to-blood ratios over time, reaching 1.13 ± 0.29, 3.67 ± 0.29, 4.10 ± 0.42 and 3.53 ± 1.03, respectively, at 6, 24, 48 and 72 h.

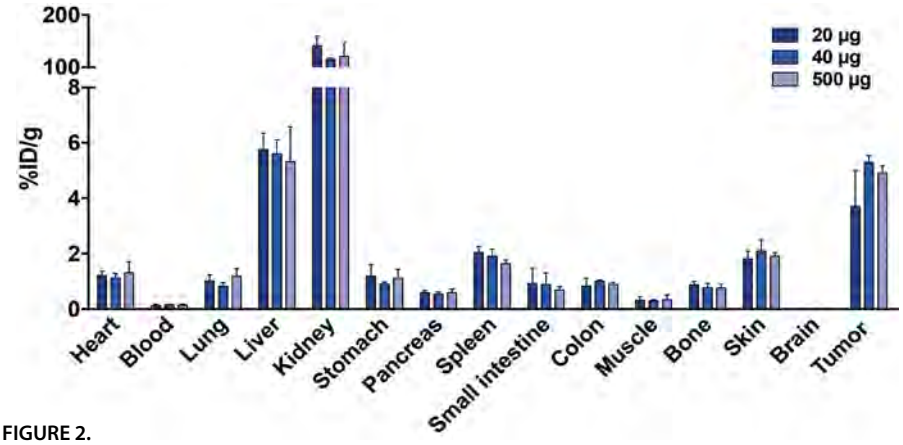

FIGURE 2.

Dose-dependent ^{89}Zr-AMG 110 biodistribution in HT-29 tumor-bearing mice at 24 h after tracer injection. Mice were injected with 20- (n = 5), 40- (n = 4), or 500-µg (n = 3) protein doses. No significant differences were observed in organ and tumor uptake between dose groups. Data are mean ± SD.

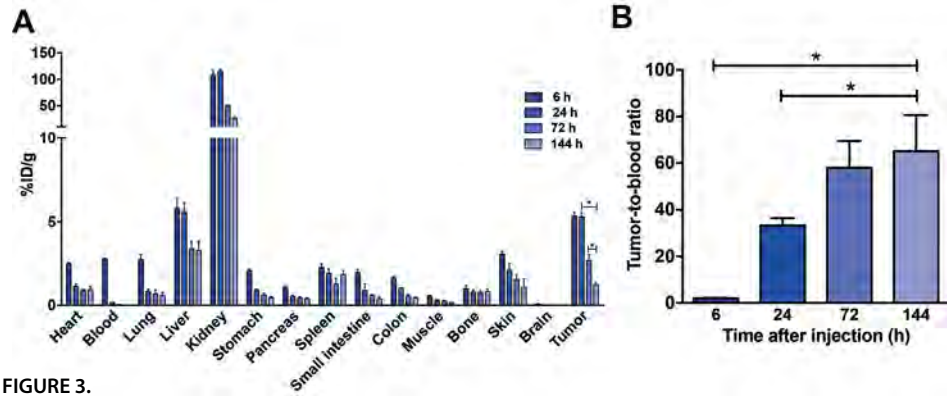

FIGURE 3.

Time-dependent ^{89}Zr-AMG 110 (40 µg) biodistribution in HT-29-bearing mice. (**A**) *Ex vivo* biodistribution of ^{89}Zr-AMG 110 was performed at 6 (n = 3), 24 (n = 4), 72 (n = 4), and 144 h (n = 5) after injection. (**B**) Corresponding tumor-to-blood ratios increased significantly. Data are mean ± SD. Significance has been calculated for differences in tumor uptake and tumor-to-blood ratios. * $P \leq 0.05$.

A 40- μg and 500-μg protein dose resulted in a higher (not statistically significant) and more reproducible tumor uptake of ^{89}Zr-AMG 110 than 20 μg (5.30 ± 0.21 and 4.9 ± 0.21 vs. 3.6 ± 1.2 %ID/g; P = 0.57 and 0.75 respectively, Fig. 2A). No statistical significant differences were found in tumor-to-blood or tumor-to-muscle ratio among the different protein doses tested (Supplementary Figs. 5A and 5B). All organs showed similar ^{89}Zr-AMG 110 levels at all protein doses. Highest ^{89}Zr-AMG 110 levels were found in the kidneys followed by liver and tumor. Because of a more reproducible tumor uptake, the remainder of the study was performed with a 40- instead of 20-μg dose level.

The duration and level of ^{89}Zr-AMG 110 tumor exposure was protein-dose-dependent and differed from blood. Biodistribution of 40 μg of ^{89}Zr-AMG 110 in time resulted in a maximum tumor uptake at 6 and 24 h after injection of 5.4 ± 0.2 %ID/g and 5.3 ± 0.3 %ID/g, respectively (Fig. 3A), declining subsequently. In contrast, tumor uptake after injection of 20 μg ^{89}Zr-AMG 110 already peaked at 6 h and declined steadily thereafter (Fig. 1B). The biologic half-life of ^{89}Zr-AMG 110 after injection of a protein dose of 40 μg in blood was 4.1 h compared with 1.5 h for the 20-μg protein dose (Supplementary Fig. 4C). Washout of signal from the tumor was relatively slow compared with blood (half-life, 40.2 h; Supplementary Fig. 4D). The prolonged tumor retention of 40 μg of ^{89}Zr-AMG 110 resulted in increasing tumor-to-blood ratios over time, reaching 65.1 ± 15.5 at 144 h (Fig. 3B). The maximal tumor-to-muscle ratio was reached at 24 h (18.6 ± 3.6).

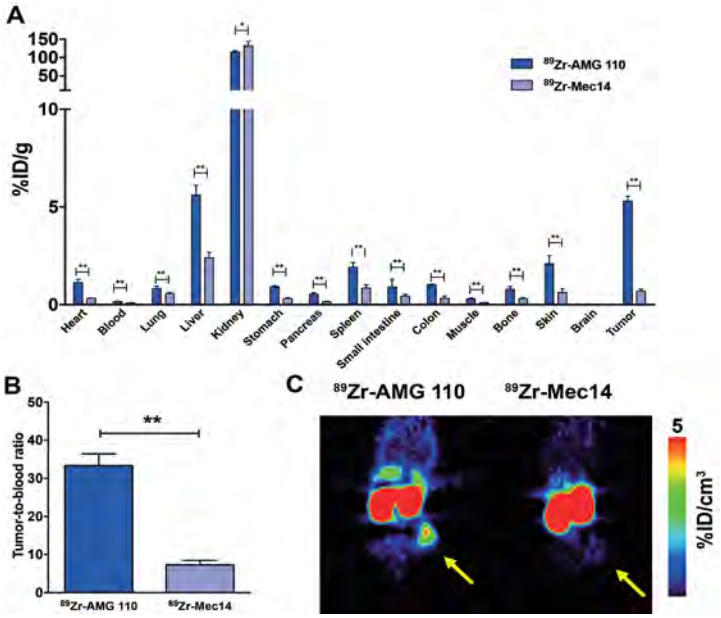

FIGURE 4.

(**A**) *Ex vivo* biodistribution 24 h after injection of ^{89}Zr-AMG 110 (40 μg, n = 4) or ^{89}Zr-Mec14 (40 μg, n = 6) in HT-29-tumor bearing mice. (**B**) Corresponding tumor-to-blood ratios were significantly higher for ^{89}Zr-AMG 110 than for ^{89}Zr-Mec14. (**C**) Representative coronal small-animal PET images of ^{89}Zr-AMG 110 and ^{89}Zr-Mec14 visualize difference in tumor uptake. Yellow arrow indicates tumor. Data are mean ± SD. *$P \leq 0.05$. ** $P \leq 0.01$.

HT-29 xenografts specifically retained ^{89}Zr-AMG 110, but not the non-EpCAM binding ^{89}Zr-Mec14 BiTE. Biodistribution of ^{89}Zr-Mec14 showed low tumor uptake of 0.7 ± 0.1 %ID/g compared with 5.3 ± 0.3 %ID/g for ^{89}Zr-AMG 110 at 24 h (Fig. 4A; $P < 0.01$). Accumulation of ^{89}Zr-Mec14 in blood and all organs except the kidneys was lower (≤ 2.4 %ID/g) than ^{89}Zr-AMG 110 (≤ 5.6 %ID/g). ^{89}Zr-Mec14 tumor uptake was comparable to nonspecific uptake in other organs. As a result, a higher tumor-to-blood (33.4 ± 3.1 vs. 7.3 ± 1.2; $P < 0.01$; Fig. 4B) and a higher tumor-to-muscle ratio (18.6 ± 3.6 vs. 6.7 ± 0.8; $P < 0.01$) were observed for ^{89}Zr-AMG 110. In line with these results, small-animal PET images showed lower tumor uptake of ^{89}Zr-Mec14 than ^{89}Zr-AMG 110 (Fig. 4C).

Tumor uptake of ^{89}Zr-AMG 110 was correlated with the level of cell surface EpCAM expression (Fig. 5). It was highest in HT-29 tumors (5.3 ± 0.3 %ID/g) followed by FaDu (2.7 ± 0.6 %ID/g) and HL-60 (0.8 ± 0.2 %ID/g), whereas no differences were observed in uptake of normal organs in mice bearing the different tumor xenografts (Fig. 5A). Difference in tumor uptake could be clearly visualized by small-animal PET (Fig. 5B).

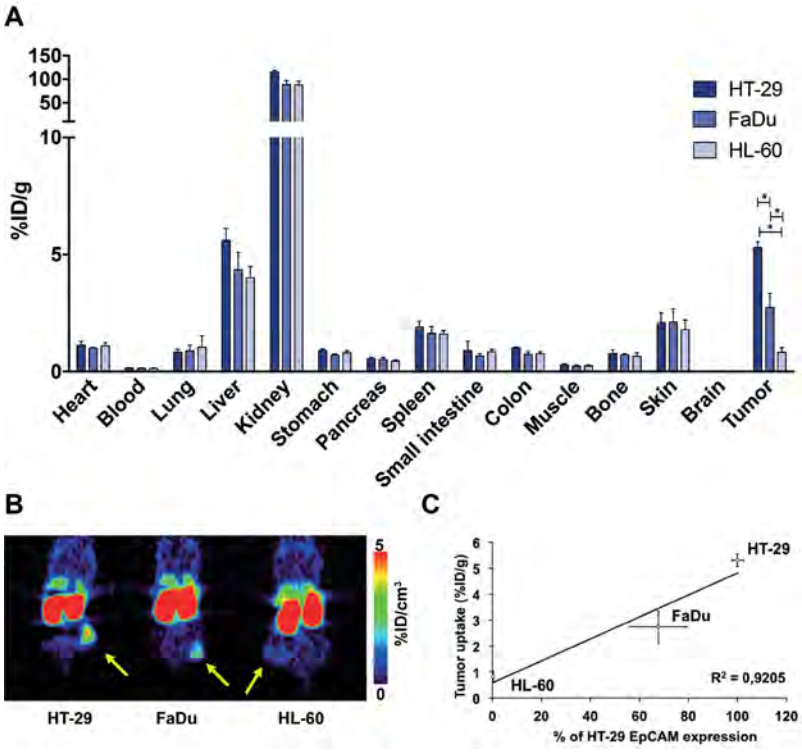

FIGURE 5.
Correlation between ^{89}Zr-AMG 110 tumor uptake and EpCAM expression on tumor cells. (**A**) *Ex vivo* biodistribution of ^{89}Zr-AMG 110 (40 µg) 24 h after tracer injection in mice bearing HT-29 ($n = 4$; high EpCAM), FaDu ($n = 5$; intermediate EpCAM), or HL-60 ($n = 6$; EpCAM-negative) cells. (**B**) Representative coronal small-animal PET images. Yellow arrows indicate tumor. (**C**) Differences in EpCAM expression on HT-29 ($n = 5$), FaDu ($n = 5$), and HL-60 ($n = 4$) cells correlated with tumor uptake of ^{89}Zr-AMG 110. Data are mean ± SD. *$P \leq 0.05$.

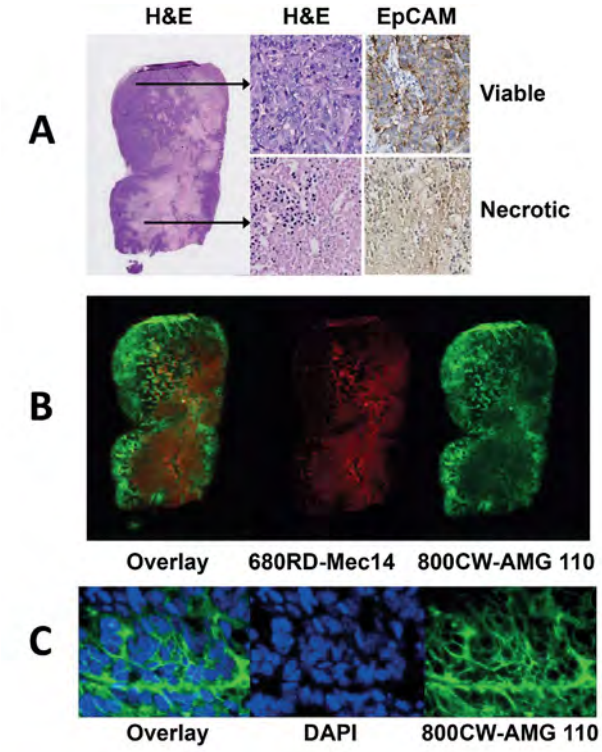

FIGURE 6.
Intratumoral distribution of coinjected 800CW-AMG 110 (40 µg) and 680RD-Mec14 (40 µg) in HT-29 tumors. (**A**) EpCAM was predominantly expressed on healthy tumor tissue as visualized with hematoxylin and eosin (H&E) and EpCAM immunohistochemical staining. (**B**) Corresponding macroscopic fluorescent imaging of 800CWAMG 110 (green) and 680RD-Mec14 (red) distribution, with minor overlapping signal (yellow). (**C**) Fluorescence microscopy images (630x), visualizing membrane localization of 800CW-AMG 110 (green) and DAPI stained nuclei (blue).

In vivo and *ex vivo* fluorescence imaging confirmed AMG 110-specific cell surface binding of HT-29 xenografts. Similar to ^{89}Zr-AMG 110, *in vivo* imaging showed HT-29 retention of 800CW-AMG 110, but not 680RD-Mec14 (Supplementary Fig. 6A). In accordance with low tumor levels found for ^{89}Zr-Mec14 at biodistribution 24 h after tracer injection, 680RD-Mec14 was cleared rapidly, with level detectable only *ex vivo* by 24 h (Supplementary Fig. 6B). *Ex vivo* macroscopic fluorescence imaging of HT-29 tumor slices showed 800CW-AMG 110 colocalizing with viable EpCAM-expressing tumor tissue, as shown by hematoxylin and eosin and EpCAM staining (Figs. 6A and 6B). Fluorescence microscopy also showed presence of 800CW-AMG 110 on the tumor cell surface (Fig. 6C). In contrast, non-EpCAM binding 680RD-Mec14 mostly localized in necrotic tumor tissue.

DISCUSSION

We present the first, to our knowledge, noninvasive preclinical imaging study in which a bispecific T cell-engaging antibody construct targeting EpCAM is labeled with a radionuclide, or a fluorophore, to visualize and quantify tumor uptake, tissue accumulation and clearance kinetics *in vivo*. In this study, ^{89}Zr-AMG 110 showed consistent tumor uptake in xenografts that is correlated with EpCAM expression. It also showed prolonged tumor retention that is unusual for a reversible extracellular binding exhibiting rapid renal clearance.

Remarkably, HT-29 tumor uptake of ^{89}Zr-AMG 110 remained visible up to 72 h after injection, despite minimal cellular internalization. Both tumor uptake and organ uptake of ^{89}Zr-AMG 110 was higher than of ^{89}Zr-Mec14, likely the result of faster clearance of ^{89}Zr-Mec14, because blood levels of ^{89}Zr-Mec14 were also lower. NIR fluorescent imaging with 800CW-AMG 110 confirmed AMG 110 localization at the tumor cell membrane in viable HT-29 tumor tissue. Minor accumulation of 680RD-Mec14 was observed in necrotic tumor tissue, which is likely due to nonspecific binding. Together, these findings clearly demonstrate the advantage of using immuno-PET to determine the dose level of BiTE antibody constructs necessary for tumor targeting, to assess the presence of target, and to study *in vivo* tissue exposure in real time.

AMG 110 showed favorable tumor uptake and retention compared with a similar EpCAM binding agent. The EpCAM-targeting radiopharmaceutical ^{68}Ga-scFv$^{42}_{9}$ also comprises 2 scFv fragments and has a molecular weight (51.2 kDa) similar to ^{89}Zr-AMG 110.[15] Furthermore, it exhibits monospecific bivalent binding and higher EpCAM affinity than AMG 110 (dissociation constant = 0.24 vs. 170-230 nM, respectively, as determined by plasmon resonance analysis).[10] Despite bivalent binding and higher affinity, the highest tumor uptake (in %ID/g) of ^{68}Ga-scFv$^{42}_{9}$ in HT-29 tumors was 2.8-fold lower than ^{89}Zr-AMG 110.[16]Maximum tumor uptake of ^{68}Ga-scFv$^{42}_{9}$ was reached at 1 h, whereas maximum tumor uptake of ^{89}Zr-AMG 110 was reached at 6 h after injection. At these time points, the observed tumor-to-blood ratios were comparable (~1 and 1.1 ± 0.30, respectively). The higher tumor uptake of ^{89}Zr-AMG 110 is most likely due to its longer circulating half-life (1.4-4.1 h) than that of ^{68}Ga-scFv$^{42}_{9}$ (0.97 h).

In addition to differences in tumor uptake kinetics and circulating half-life, preclinical imaging studies also showed that different tracers also vary in the ability to saturate tumor uptake. In contrast to membrane tumor targets c-MET and human epidermal growth factor receptor 3, saturation of EpCAM binding on HT-29 was not observed even when the ^{89}Zr-AMG 110 total protein dose was increased to 500 μg.[17,18] Thurber et al. also observed no saturation of EpCAM binding in HT-29 xenografts after injection of an EpCAM antibody labeled with a NIR dye (VivoTag 680) at a total protein dose of 180 μg.[14] One possible explanation might be related to the abundance of cell surface EpCAM on HT-29 cells (2.3 x 10^6 receptors/cell).[14] Another example supporting this hypothesis was illustrated by the lack of tumor saturation observed for ^{89}Zr-trastuzumab, up to 500 μg in SKOV3-xenografted mice.[19] Similar to the high level of EpCAM expression on HT-29 cells, expression of the human epidermal growth factor receptor 2 on SKOV3 cells is also high (6.6 x 10^6 receptors/cell).[20] The inability to saturate human epidermal growth factor receptor 2 and EpCAM suggest that it may be difficult to saturate receptors when their cell surface expression exceeds approximately 2 x 10^6 receptors/cell at the dose levels evaluated. Alternatively, saturation of tumor targets may also depend on their *in vivo* properties of the antibodies including binding on/off kinetics, degree of tumor penetration, and access targets at different protein dose levels.

Additional radioactive- and optical-labeled antibody imaging studies, particularly those in the clinical setting, will help further elucidate mechanisms for driving uptake in tumors and tissues of interest.

Although the current preclinical study examined only the tumor antigen-binding component of AMG 110, preclinical and clinical imaging studies showed that it is feasible to image tumor uptake of tumor-targeting CD3-bispecific antibodies in the presence of circulating T cells. A T cell-mediated increase in tumor uptake has been observed with a tetravalent bispecific tandem antibody (TandAb), directed at mouse CD3ε and fibronectin extra domain B, in immunocompetent mice.[21] ^{125}I-labeled TandAb with CD3ε affinity similar to that of AMG 110 showed that potential T cell binding outside of the tumor did not block tumor uptake or change its biodistribution.[21] The mice in our study were immunodeficient, so tumor uptake of ^{89}Zr-AMG 110 was not affected by T cells. Because AMG110 does not bind mouse CD3e, the effect of T cell binding on ^{89}Zr-AMG 110 distribution and tumor uptake could not be studied in immune-competent mice. In a clinical setting, the presence of T cells might influence biodistribution and lead to a higher tumor uptake. Furthermore, ^{123}I-OC/TR F(ab')$_2$, targeting folate receptor and CD3, has been used successfully to image malignant tumor lesions in ovarian cancer patients.[22]

CONCLUSION

Given its overexpression by many tumor types, EpCAM is an interesting drug target. Different EpCAM-targeted drugs have been developed, including monoclonal antibodies, antibody fragments, bispecific antibodies, and antibody-drug conjugates. Similar to these other experimental drugs, EpCAM expression on tumor cells is a prerequisite for effective treatment with AMG 110. Because EpCAM-dependent ^{89}Zr-AMG 110 tumor uptake has been demonstrated preclinically, this tracer, applied clinically, can potentially facilitate patient selection for AMG 110 treatment by providing information on drug access across all lesions. Moreover, ^{89}Zr-AMG 110 or other radiolabeled BiTE antibody constructs could potentially support clinical BiTE development, because they could give additional information about tissue pharmacokinetics and uptake in tumors to support optimal dosing and about uptake in critical organs to anticipate toxicity.

REFERENCES

1. *Gao J, Bernatchez C, Sharma P, et al. Advances in the development of cancer immunotherapies. Trends Immunol. 2013;34:90-8.*
2. *Stewart TJ, Smyth MJ. Improving cancer immunotherapy by targeting tumor-induced immune suppression. Cancer Metastasis Rev. 2011;30:125-40.*
3. *Garcia-Lora A, Algarra I, Garrido F. MHC class I antigens, immune surveillance, and tumor immune escape. J Cell Physiol. 2003;195:346-55.*
4. *Frankel SR, Baeuerle PA. Targeting T cells to tumor cells using bispecific antibodies. Curr Opin Chem Biol. 2013;17:385-92.*

5. *Offner S, Hofmeister R, Romaniuk A, et al. Induction of regular cytolytic T cell synapses by bispecific single-chain antibody constructs on MHC class I-negative tumor cells. Mol Immunol. 2006;43:763-71.*
6. *Dreier T, Baeuerle PA, Fichtner I, et al. T cell costimulus-independent and very efficacious inhibition of tumor growth in mice bearing subcutaneous or leukemic human B cell lymphoma xenografts by a CD19-/CD3-bispecific single-chain antibody construct. J Immunol. 2003;170:4397-402.*
7. *Haas C, Krinner E, Brischwein K, et al. Mode of cytotoxic action of T cell-engaging BiTE antibody MT110. Immunobiology. 2009;214:441-53.*
8. *Petsch S, Gires O, Rüttinger D, et al. Concentrations of EpCAM ectodomain as found in sera of cancer patients do not significantly impact redirected lysis and T-cell activation by EpCAM/CD3-bispecific BiTE antibody MT110. MAbs. 2011;3:31-7.*
9. *Went PTH, Lugli A, Meier S, et al. Frequent EpCAM protein expression in human carcinomas. Hum Pathol. 2004;35:122-8.*
10. *Brischwein K, Schlereth B, Guller B, et al. MT110: a novel bispecific single-chain antibody construct with high efficacy in eradicating established tumors. Mol Immunol. 2006;43:1129-43.*
11. *Fiedler WM, Wolf M, Kebenko M, et al. A phase I study of EpCAM/CD3-bispecific antibody (MT110) in patients with advanced solid tumors [abstract]. J Clin Oncol. 2012;30(15, suppl):2504.*
12. *Lamberts LE, Williams SP, Terwisscha van Scheltinga AGT, et al. Antibody positron emission tomography imaging in anticancer drug development. J Clin Oncol. 2015;33:1491-504.*
13. *Terwisscha van Scheltinga AGT, van Dam GM, Nagengast WB, et al. Intraoperative near-infrared fluorescence tumor imaging with vascular endothelial growth factor and human epidermal growth factor receptor 2 targeting antibodies. J Nucl Med. 2011;52:1778-85.*
14. *Thurber GM, Weissleder R. Quantitating antibody uptake in vivo: conditional dependence on antigen expression levels. Mol Imaging Biol. 2011;13:623-32.*
15. *Choi BD, Cai M, Bigner DD, et al. Bispecific antibodies engage T cells for antitumor immunotherapy. Expert Opin Biol Ther. 2011;11:843-53.*
16. *Eder M, Knackmuss S, Le Gall F, et al. ^{68}Ga-labelled recombinant antibody variants for immuno-PET imaging of solid tumours. Eur J Nucl Med Mol Imaging. 2010;37:1397-407.*
17. *Terwisscha van Scheltinga AGT, Lub-de Hooge MN, Hinner MJ, et al. In vivo visualization of MET tumor expression and anticalin biodistribution with the MET-specific anticalin ^{89}Zr-PRS-110 PET tracer. J Nucl Med. 2014;55:665-71.*
18. *Terwisscha van Scheltinga AGT, Lub-de Hooge MN, Abiraj K, et al. ImmunoPET and biodistribution with human epidermal growth factor receptor 3 targeting antibody ^{89}Zr-RG7116. MAbs. 2014;6:1051-58.*
19. *Dijkers ECF, Kosterink JGW, Rademaker AP, et al. Development and characterization of clinical-grade ^{89}Zr-trastuzumab for HER2/neu immunoPET imaging. J Nucl Med. 2009;50:974-81.*
20. *DeFazio-Eli L, Strommen K, Dao-Pick T, et al. Quantitative assays for the measurement of HER1-HER2 heterodimerization and phosphorylation in cell lines and breast tumors: applications for diagnostics and targeted drug mechanism of action. Breast Cancer Res. 2011;13:R44.*
21. *List T, Neri D. Biodistribution studies with tumor-targeting bispecific antibodies reveal selective accumulation at the tumor site. MAbs. 2012;4:775-83.*
22. *Tibben JG, Boerman OC, Massuger LFAG, et al. Pharmacokinetics, biodistribution and biological effects of intravenously administered bispecific monoclonal antibody OC/TR F(ab')$_2$ in ovarian carcinoma patients. Int J Cancer. 1996;66:477-83.*

DISCLOSURE

The costs of publication of this article were defrayed in part by the payment of page charges. Therefore, and solely to indicate this fact, this article is hereby marked "advertisement" in accordance with 18 USC section 1734.

This work was supported by Amgen and ERC advanced grant 293445 (OnQview). Matthias Friedrich, Petra Deegen, Sabine K. Stienen, Pete C. Pieslor, and Hung K. Cheung are employed by Amgen and have ownership interest (including patents) in AMGEN. No other potential conflict of interest relevant to this article was reported.

SUPPLEMENTARY DATA

SUPPLEMENTARY MATERIALS AND METHODS

Conjugation and labeling of AMG 110 and Mec14

AMG 110 and Mec14 were first purified with water for injections using a Vivaspin-2 10 kDa filter (GE Healthcare). Conjugation was performed by allowing BiTE antibody constructs to react with a 6.7-fold molar excess of *N*-succinyldesferrioxamine-B-tetrafluorphenol (*N*-suc-Df-TFP, ABX), as described earlier.[1] Conjugated BiTE was radiolabeled on the same day with ^{89}Zr-oxalate (PerkinElmer). Free ^{89}Zr was removed by using a Vivaspin-2 10 kDa filter. For labeling with respectively IRDye 800CW and 680RD, purified AMG 110 and Mec14 reacted with a 3-fold molar excess of IRDye as described earlier.[2] Unreacted dye was removed using PD10 desalting columns (Fisher Scientific).

Quality control of ^{89}Zr-AMG 110 and ^{89}Zr-Mec14

Aggregation, fragmentation and concentration of ^{89}Zr-AMG 110, 800CW-AMG 110, ^{89}Zr-Mec14 and 680RD-Mec14 were assessed using size exclusion high performance liquid chromatography (SE-HPLC). The Waters SE-HPLC system was equipped with a dual wavelength absorbance detector, an in line radioactivity detector and a size exclusion column (Superdex 75 10/300 GL column; GE Healthcare). PBS was used as mobile phase at a flow of 0.7 ml/min. Radiochemical purity (RCP) of ^{89}ZrAMG 110 and ^{89}Zr-Mec14 was determined using trichloroacetic acid precipitation.[3]

The *in vitro* binding characteristics (immunoreactive fraction; IRF) of the radiolabeled BiTE antibody constructs were determined in a cell binding assay as described by Lindmo et al.4 In short, two series of HT-29 cell dilutions were incubated in duplicate with 15 ng/mL ^{89}Zr-AMG 110 for 2 h at 4°C while shaking. To one of the cell series a 1000 fold excess of cold AMG 110 was added to block EpCAM specific binding and set the reference used to correct for non-specific binding. After 2 h incubation, cells were washed twice with PBS containing 1% human serum albumin (HSA). Radioactivity of standards and cell pellets were measured with a calibrated well-type γ-counter (LKB 1282; CompuGamma). The IRF was determined for each separate experiment by extrapolating to conditions representing infinite antigen excess, corrected for non-specific binding.

In vitro evaluation of ^{89}Zr-AMG 110

Internalization of ^{89}Zr-AMG 110 was determined by incubating 10^6 HT-29 cells with 50 ng ^{89}Zr-AMG 110 for 1 h at 4°C. Subsequently, unbound ^{89}Zr-AMG 110 was removed by rinsing with PBS containing 1% HSA. Remaining activity, defined as initial cell associated radioactivity, was measured in a calibrated well-type γ-counter and set to 100%. Next cells were resuspended in culture medium (RPMI + 10% FCS, including T = 0) and incubated 1, 2 or 4 h at 4°C or 37°C. Thereafter, medium was removed and cell pellet activity, defined as membrane bound + internalized, was measured in a calibrated well-type γ-counter. Finally, cells were stripped using urea buffer (4 M urea, 2 M glycine, pH 2.0)[5] and washed twice with urea buffer. Radioactivity in the stripped pellet, representing the internalized radioactivity, was measured in a calibrated welltype γ-counter. Internalization was determined by the following formula: (internalized radioactivity/initial cell associated radioactivity) x 100%.

Flow cytometry

To determine EpCAM expression by the cell lines, flow cytometry was performed with a BD Accuri™ C6 flow cytometer (BD Biosciences). HT-29, FaDu or HL-60 cells were incubated for 1 h at 4 °C, with 20 μg/mL mouse anti-human EpCAM antibody (Abcam, ab20160) and washed twice using phosphate buffered saline (PBS; 140 mmol/L NaCl, 9 mmol/L Na_2HPO_4, 1.3 mmol/L NaH_2PO_4; pH = 7.4, UMCG) containing 0.5% FCS and 2 mM ethylenediaminetetraacetic acid. Subsequently, cells were incubated for 1 h at 4°C with (0.01 mg/mL) goat anti-mouse phycoerythrin secondary antibody (Southern Biotech). Cells were finally washed twice and EpCAM expression was assessed. Membrane expression was calculated as mean fluorescent intensity and expressed as percentage of HT-29.

In vivo fluorescent imaging

For NIR fluorescence imaging, mice bearing HT-29 xenografts (n = 4) were coinjected with 40 μg 800CW-AMG 110 and 40 μg 680RD-Mec14. Mice undergoing fluorescent imaging were kept on an alfalfa-free diet to minimize autofluorescence. Imaging was performed at 0.5, 1, 3, 6 and 24 h after tracer injection, using the IVIS Spectrum (Caliper Life Sciences) imaging system. Excitation wavelengths were set at 640 nm for 680RD-Mec14 and 745 nm for 800CW-AMG 110. Data were analyzed using Living Image 3.2 software (Caliper Life Sciences). Tumor signal was

determined by drawing regions of interest around tumor boundaries for both 680RD-Mec14 and 800CW-AMG 110.

SUPPLEMENTARY RESULTS

Labeling and quality control of ^{89}Zr-AMG 110 and ^{89}Zr-Mec14

AMG 110 and Mec14 were successfully conjugated with *N*-suc-Df-TFP (ratio 1:3) and labeled with ^{89}Zr. The retention time for AMG 110 and Mec14 was approximately 17 min. ^{89}Zr-*N*-suc-Df-TFP, low-molecular-weight impurities and buffer additives eluted around 25 min on the SE-HPLC (Supplementary Fig 2A). Upon *N*-suc-Df-TFP conjugation and ^{89}Zr labeling of AMG 110 and Mec14, SE-HPLC did not show aggregation or fragmentation and radiochemical purity was confirmed using trichloroacetic acid precipitation tests (respectively 96.8 ± 1.1% and 96.2%; $n = 10$ and $n = 1$).

Conjugation of *N*-suc-Df-TFP to AMG 110 and subsequent labeling with ^{89}Zr resulted in a mean IRF of 0.60 ± 0.03 for EpCAM (Supplementary Figs. 2B and 2C; $n = 6$). Subsequent to EpCAM binding, ^{89}Zr-AMG 110 showed minimal internalization by HT-29 cells at 37°C *in vitro* (Supplementary Fig. 3).

SUPPLEMENTARY REFERENCES

1. *Verel I, Visser GWM, Boellaard R, et al. ^{89}Zr immuno-PET: Comprehensive procedures for the production of ^{89}Zr-labeled monoclonal antibodies. J Nucl Med. 2003;44:1271-81.*
2. *Terwisscha van Scheltinga AGT, van Dam GM, Nagengast WB, et al. Intraoperative near-infrared fluorescence tumor imaging with vascular endothelial growth factor and human epidermal growth factor receptor 2 targeting antibodies. J Nucl Med. 2011;52:1778-85.*
3. *Nagengast WB, de Vries EGE, Hospers GA, et al. In vivo VEGF imaging with radiolabeled bevacizumab in a human ovarian tumor xenograft. J Nucl Med. 2007;48:1313-19.*
4. *Lindmo T, Boven E, Cuttitta F, et al. Determination of the immunoreactive fraction of radiolabeled monoclonal antibodies by linear extrapolation to binding at infinite antigen excess. J Immunol Methods. 1984;72:77-89.*
5. *Oude Munnink TH, de Vries EGE, Vedelaar SR, et al. Lapatinib and 17AAG reduce ^{89}Zr-trastuzumab-F(ab')$_2$ uptake in SKBR3 tumor xenografts. Mol Pharm. 2012;9:2995-3002.*

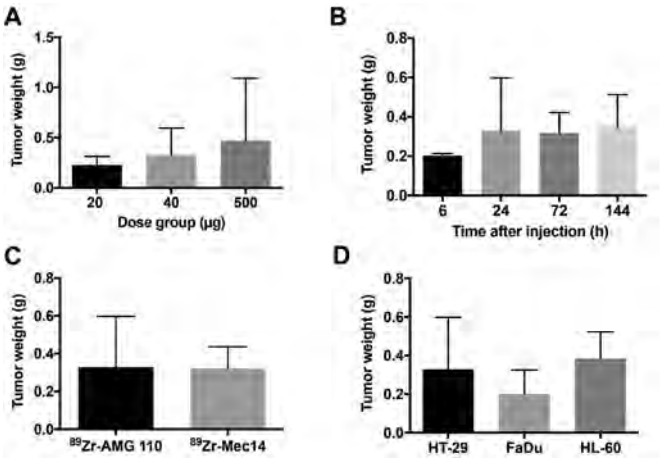

SUPPLEMENTARY FIGURE 1.

Differences in *ex vivo* tumor weights between the experiments, as measured after mice were sacrificed. (**A**) Difference in tumor weights after resection from mice injected with ^{89}Zr-AMG 110 at 20 µg (n = 5), 40 µg (n = 4) or 500 µg (n = 3) dose levels. (**B**) Difference in tumor weights at 6 (n = 3), 24 (n = 4), 72 (n = 4) and 144 h (n = 5) after injection of 40 µg ^{89}Zr-AMG 110. (**C**) Difference in tumor weights at 24 h after injection of 40 µg ^{89}Zr-AMG 110 (n = 4) or 40 µg ^{89}Zr-Mec 14 (n = 6). (**D**) Difference in tumor weights between HT-29 (n = 4), FaDu (n = 5) and HL-60 (n = 6) tumors at 24 h after injection of 40 µg ^{89}Zr-AMG 110.

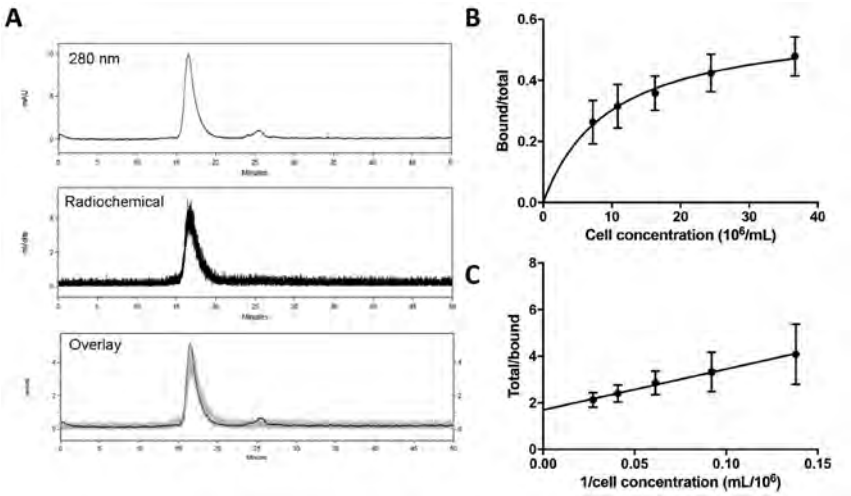

SUPPLEMENTARY FIGURE 2.

Quality control of ^{89}Zr-AMG 110 and ^{89}Zr-Mec 14. Panel (**A**) shows a typical SE-HPLC chromatogram of ^{89}Zr-AMG 110 (upper panel) or ^{89}Zr-Mec 14 (lower panel), which is an overlay of 280 nm and radiochemical signal. The binding of ^{89}Zr-AMG 110 to an increasing number of HT-29 cells is shown in panel (**B**). Its reciprocal plot to infinite antigen excess was used to determine immunoreactive fraction in panel (**C**). Data is presented as mean ± SD.

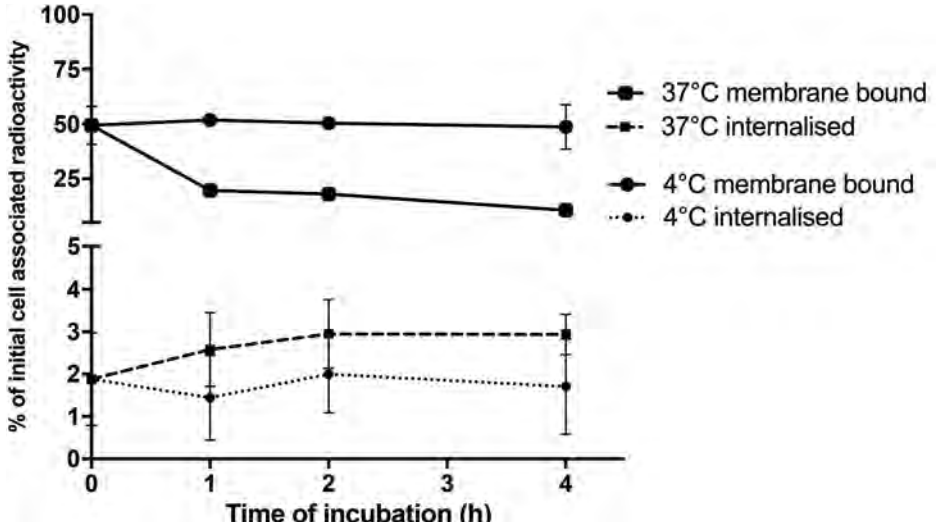

SUPPLEMENTARY FIGURE 3.
Membrane binding and internalization of ^{89}Zr-AMG 110 after binding EpCAM on HT-29 cells. Membrane bound and internalized fraction is expressed as percentage of initial cell associated radioactivity. Data is presented as mean ± SD. At several time points in the graphs of membrane bound ^{89}Zr-AMG 110, SD is not visible due its small size.

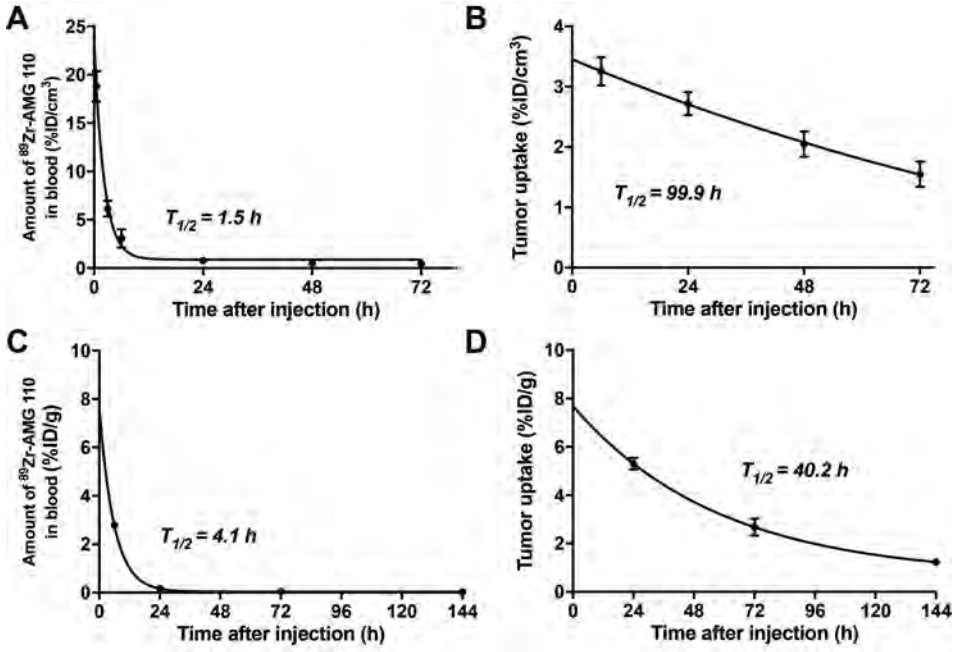

SUPPLEMENTARY FIGURE 4.
Membrane binding and internalization of ^{89}Zr-AMG 110 after binding EpCAM on HT-29 cells. Membrane bound and internalized fraction is expressed as percentage of initial cell associated radioactivity. Data is presented as mean ± SD. At several time points in the graphs of membrane bound ^{89}Zr-AMG 110, SD is not visible due its small size.

49

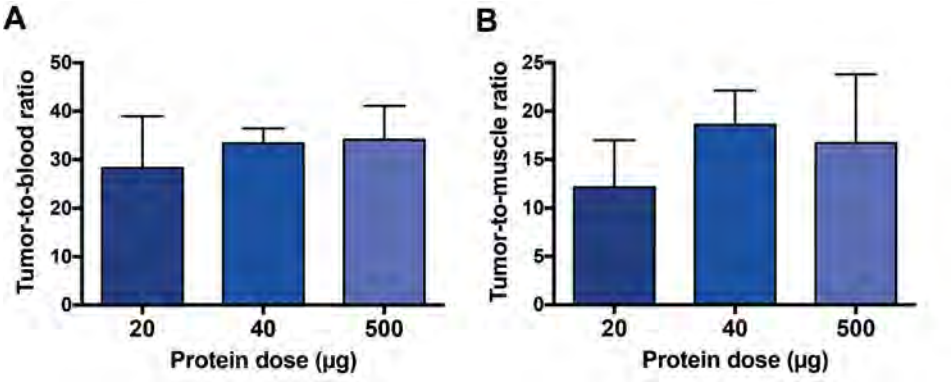

SUPPLEMENTARY FIGURE 5.
Dose dependent tumor-to-blood (**A**) and tumor-to-muscle ratios (**B**). Mice were injected with 20 µg (n = 5), 40 µg (n = 4) or 500 µg (n = 3) protein doses. No significant differences were observed in blood or tissue levels between the dose groups. Data is presented as mean ± SD.

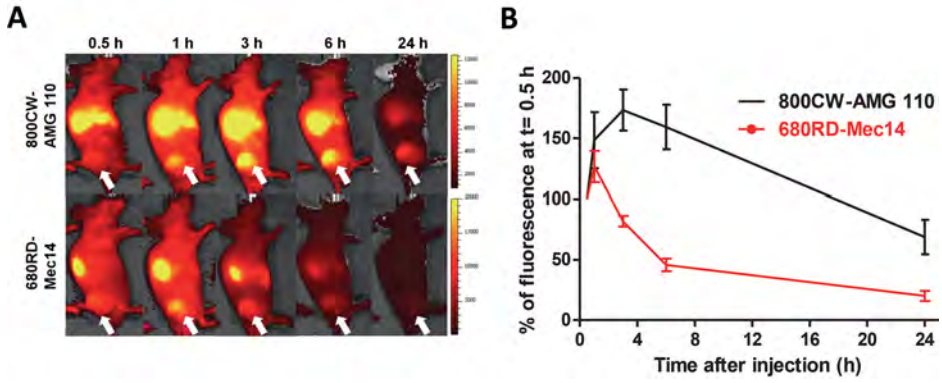

SUPPLEMENTARY FIGURE 6.
(**A**) Representative sagittal two-dimensional *in vivo* fluorescence images at indicated time points, after coinjection of 40 µg 800CW-AMG 110 and 40 µg 680RD-Mec14. White arrow indicates location of the tumor. (**B**) Fluorescent tracer uptake in HT-29 tumors over time, normalized to absolute fluorescence levels at 30 min after tracer injection. Data is presented as mean ± SD.